A Prominin-1–Rich Pediatric Glioblastoma: Biologic Behavior Is Determined by Oxygen Tension–Modulated CD133 Expression but Not Accompanied by Underlying Molecular Profiles[1,2]

Laura K. Donovan*, Nicola E. Potter[†], Tracy Warr[‡] and Geoffrey J. Pilkington*

*Cellular and Molecular Neuro-oncology Group, Institute of Biomedical and Biomolecular Sciences, School of Pharmacy and Biomedical Sciences, University of Portsmouth, Portsmouth, UK; [†]Department of Molecular Neuroscience, Institute of Neurology, University College London, National Hospital for Neurology and Neurosurgery, London, UK; [‡]Brain Tumour UK Neuro-oncology Research Group, Research Institute in Healthcare Sciences, School of Applied Sciences, University of Wolverhampton, Wolverhampton, UK

Abstract

Few studies on the biologic and molecular properties of pediatric glioblastoma have been performed. Until now, differential genomic analysis of CD133^{+}ve and CD133^{−}ve fractions has not been described in pediatric glioma. We hypothesize not only that the presence of CD133 could be the source of tumor resistance but also that maintenance of this molecule by hypoxia dictates cellular and molecular behavior. From a series of human glioblastoma biopsies investigated, only one, IN699 (from a pediatric glioblastoma), generated greater than 4% of the total cell volume as CD133^{+}ve cells. Using this pediatric glioblastoma, containing unprecedented high levels of the putative brain tumor stem cell marker CD133, as a study model, we report biologic and molecular characteristics of the parent culture and of CD133^{+}ve and CD133^{−}ve populations derived therefrom under atmospheric and hypoxic culture conditions. Immunocytochemistry and flow cytometry were performed with antigenic markers known to characterize neural stem cells and associated glioma behavior. Behavioral analysis was carried out using proliferation, adhesion, migration, and invasion assays. Cell cycle analysis and array comparative genomic hybridization were used to assess copy number profiles for parental cells and CD133^{+}ve and CD133^{−}ve fractions, respectively. With regard to invasion and proliferation, CD133^{+}ve and CD133^{−}ve fractions were inversely proportional, with a significant increase in invasive propensity within the CD133^{−}ve cells ($P < .005$) and a significant increase in proliferation within CD133^{+}ve cells ($P < .005$). Our observations indicate identical genomic imbalances between CD133^{+}ve and CD133^{−}ve fractions. Furthermore, our research documents a direct link between decreasing oxygen tension and CD133 expression.

Translational Oncology (2012) 5, 141–154

Introduction

Although brain tumors are the most common solid cancers in children, relatively few studies have been performed on the biological and molecular properties of pediatric glioblastoma (GB). Unlike adult GB, very little is understood about the mechanisms of tumorigenesis in pediatric GB. The cell of origin within pediatric brain tumors (PBTs) is often unclear [1]. One theory is that PBTs occur from the transformation of proliferating neural stem cells (NSCs) [2]. Several lines of evidence support this theory; first, PBTs are frequently

made of multiple cell types, suggesting that they originate from cells with multilineage potential [3]; second, several PBTs seem to arise from the subventricular zone, the region of the brain harboring NSCs [4]; and third, PBTs regularly overexpress genes required to regulate the self-renewal and proliferation of NSCs [5] or typically display mutations within these regulatory genes [1]. If PBTs do indeed contain cells displaying stem cell characteristics, it is crucial to know whether these cells also harbor aberrant properties critical for the abnormal growth of the tumor [1].

Several groups have identified the existence of a highly tumorigenic subset of brain tumor cells. Studies have demonstrated a clear association between this subset and (i) the expression of stem cell markers such as Sox-2, Musashi-1, oligodendrocyte transcription marker 2 (Olig-2), and Nestin; (ii) the ability to undergo multipotent cellular differentiation; and (iii) the capacity to generate neurospheres. CD133 (prominin-1) is a 120-kDa-transmembrane-spanning glycoprotein consisting of six domains: two N-glycosylated extracellular loops, two intracellular loops, a cytoplasmic C-terminal domain, and an extracellular N-terminal domain [6]. CD133 was originally identified as a cancer stem cell (CSC) marker in the hematopoietic system. A distinctive characteristic of this protein is its down-regulation during cellular differentiation, supported by the understanding that a cell's glycosylation state differs with alterations to the differentiation and/or malignancy state [6]. Since its first discovery, CD133, independently or in combination with other stem cell markers (such as Sox-2, Nestin, Musashi-1) has been identified in a variety of human tumors including prostate tumors, breast cancers, colon carcinomas, lung cancers, and brain tumors. Importantly, significantly higher expression levels of CD133 in GB have been associated with poor patient prognosis [7]. Furthermore, CD133-positive cells have been identified as more resistant to radiation and standard chemotherapy in comparison to CD133-negative cells [8–10]. However, the belief that CD133 may act as a universal marker of CSCs has been met with a high degree of controversy in the neuro-oncology research community, as the precise biological role of CD133 has yet to be established.

Poorly vascularized areas, associated with severe oxygen deprivation, are known to be present within solid tumors of the central nervous system (CNS) [11]. The presence of hypoxic tumor cells is thought to be a major cause of tumor cell resistance to radiotherapy [12]. The advancement of cancer by hypoxic microenvironments occurs by the initiation of transcription factors promoting cell survival, motility, and tumor angiogenesis. The cellular responses instigated by hypoxia seem to be manipulated by alterations in gene expression [13]. The stabilization of a glioma tumor cell and the cascade of events leading to this stabilization, as well as alterations in gene expression, occur through the activation of hypoxic-inducible factors (HIFs). HIFs are transcription factors crucial for the adaptive response to oxygen tension [14]. Oxygen microenvironment clearly influences stem cell development and maintenance. The most appealing hypothesis to support this finding is that stem cells may possibly benefit from hypoxic niches where oxidative DNA damage is reduced [13]. Because of the apparent complexity of the microenvironment, plus additional factors seemingly affecting the expression of the CD133 epitope, it is not surprising that there are contradictory reports in the literature regarding the functional properties and expression of CD133 [15–17].

The biologic significance of CD133 is contentious; indeed, the appropriate study model and microenvironment in which to study this molecule is debatable. We hypothesize not only that, rather than being a CSC marker *per se*, the presence of CD133 could be the source of tumor resistance but also that the maintenance of this molecule by hypoxia is linked with cellular and molecular behavioral patterns. Such a hypothesis requires a thorough understanding of the biologic behavior of CD133⁺ve and CD133⁻ve cells with increasing oxygen tensions. From a series of GB biopsies, we attempted identification and separation of CD133⁺ve cells. In all cases, with the exception of one, CD133⁺ve cells constituted less than 4% of the total cell number (data not included). The sole case, IN699 (from a pediatric GB) where levels of CD133⁺ve cells were high (40% with standard oxygen conditions and 92% with hypoxia), was used in the present study to explore the potential link between CD133 and biologic behavior. Using this pediatric GB containing unprecedented high levels of the CD133 glycoprotein as a study model, we have attempted to correlate CD133 expression with cellular phenotype and biologic behavior.

Materials and Methods

Cell Culture

IN699 is a short-term cell culture that was initiated at the Institute of Neurology, London, and derived from a supratentorial GB in a treatment-naive 15-year-old adolescent boy as previously described [18]. For the maintenance of cell culture and generation of neurospheres, cells were grown in Neurobasal A medium (NBM; Fisher Scientific, Loughborough, United Kingdom) supplemented with 20 ng/ml epidermal growth factor (Sigma-Aldrich, Dorset, United Kingdom), 20 ng/ml fibroblast growth factor 2 (Sigma-Aldrich), 32 IE/ml heparin sodium salt from porcine intestinal mucosa (Sigma-Aldrich), 10 µl/ml Glutamax (Fisher Scientific), and 20 µl/ml B27 supplement (Sigma-Aldrich). Although the cells were maintained on plastic substrate as monolayers and neurospheres (Figure 1), after high-density culture on a nonadherent substrate, the cells resembled the classic neurosphere. The cells were routinely propagated until the *in vitro* serial passage 20 was reached. Cells were either incubated at 37°C in 5% CO_2 and atmospheric O_2 (25%) in a standard humidified incubator (atmospheric conditions) or 5% CO_2 and 3% O_2 using a MiniGalaxy-A hypoxic incubator incorporating a nitrogen supply (hypoxic conditions). The appropriate oxygen tension for *in vitro* culture conditions was calculated according to the guidelines set by Csete [19] and Sullivan et al. [20]. It was ensured that exposure to atmospheric oxygen by the hypoxic cell cultures was minimal. To ensure that the parental cell culture was an appropriate model of which to investigate CD133 owing to the unprecedented high numbers of CD133⁺ve cell, an adult GB displaying between 1% and 4% of its total cell populations CD133⁺ve was used as a standard (data not shown).

Immunocytochemistry

IN699 as well as CD133⁺ve and CD133⁻ve cells derived therefrom were cultured in six-well plates and were fixed with 4% (wt/vol) paraformaldehyde for 4 minutes, washed in phosphate-buffered saline (PBS), treated with 10% normal serum for 60 minutes, and stained with a primary antibody for 60 minutes at room temperature (RT). The primary antibodies were mouse anti–ganglioside 3 (GD3) (1:150; Abcam, Cambridge, United Kingdom), mouse anti–acetylated ganglioside 3 (1:150; Invitrogen, Paisley, United Kingdom), rabbit anti–Musashi-1 (1:300; Abcam), rabbit anti–Olig-2 (1:200; Abcam), rabbit anti–Ki67 (1:100; Abcam), rabbit anti–proliferating cell nuclear antigen (PCNA, 1:200; Abcam), mouse anti–glial fibrillary
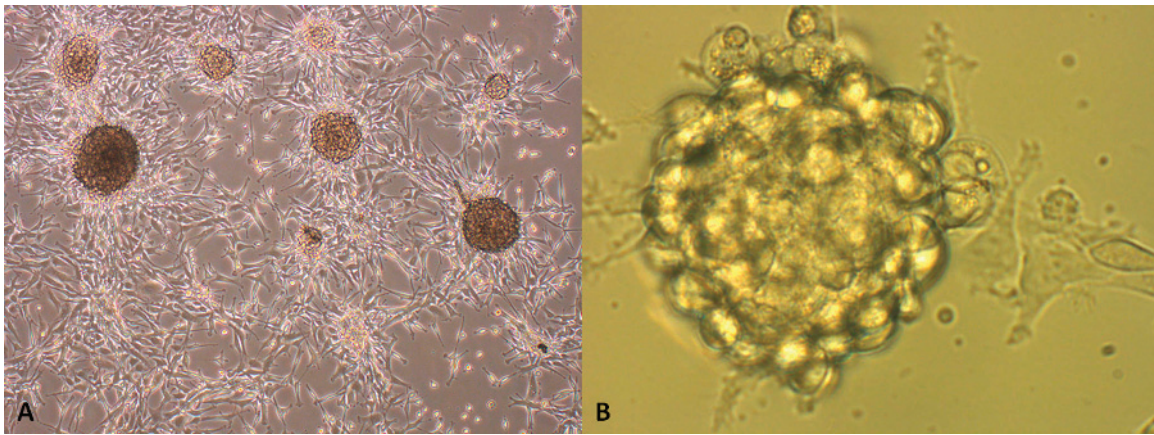
Figure 1. (A) Growth of the parental cell culture established under NSCs conditions and 3% O_2 plus 5% CO_2. When cultured under defined stem cell conditions, the parental culture forms true spheres, which are derived from a single cell, as well as some spherically aggregated clusters (B) representative of the classic neurosphere.

acidic protein (GFAP, 1:500; Dako, Cambridgeshire, United Kingdom), mouse anti–oligodendrocyte marker 4 (O4, 1:200; Sigma-Aldrich), mouse anti-Nestin (1:1000; Abcam), mouse anti–neuron-specific βIII-tubulin (1:500; Abcam), mouse anti–CD133/1 (AC133, 1:200; Miltenyi Biotec, Surrey, United Kingdom), mouse anti–HIF-1α (1:1300; Abcam), rabbit anti–HIF-2α (HIF-2α) (1:1300; Abcam), rabbit anti–SRY–related HMG BOX gene 2 (SOX2, 1:1500; Abcam), mouse anti–cluster of differentiation 15 (CD15) (1:1500; Abcam); each antibody and respective dilution factor was optimized before experimental use. Appropriate controls were used for each staining parameter. The cells were washed in PBS, incubated with the appropriate fluorochrome (1:500) for 30 minutes at RT, and treated with Hoechst Blue as the nuclear counter stain. The secondary antibodies used were goat anti–mouse immunoglobulin G (IgG) 488 (1:500; Invitrogen), goat anti–mouse IgM 488 (1:500; Invitrogen), goat anti–rabbit IgG 488 (1:500; Invitrogen), goat anti–rabbit IgG 568 (1:500; Invitrogen), and goat anti–rabbit IgM 568 (1:500; Invitrogen). Depending whether the antigenic location was intracellular or extracellular, the cells were washed in PBS and incubated for 4 minutes with 0.01% (vol/vol) Triton X-100 (Sigma-Aldrich) for membrane permeabilization. The cells were inverted and examined with a Zeiss Axio Imager upright fluorescence microscope (Carl Zeiss Ltd, Hertfordshire, United Kingdom). For sequential antigen detection, the same procedure was used as previously described for the processing of single extracellular and intracellular antigens. However, before the addition of the nuclear stain, the cells were incubated for 60 minutes at RT with 10% normal serum and subsequently processed for the second antigen.

Flow Cytometry

Cells were harvested using TryplExpress (Invitrogen) and washed in PBS. A total of 5×10^5 cells were incubated with the appropriate primary antibody (at a dilution factor outlined by the manufacturer) at 4°C for 20 minutes. The primary antibodies were mouse anti-GD3 (1:50; Abcam), mouse anti-acetylated ganglioside 3 (1:50; Invitrogen), mouse anti-CD15 (1:150; Abcam), rabbit anti–Musashi-1 (1:40; Abcam), rabbit anti–Olig-2 (1:20; Abcam), rabbit anti–Ki67 (1:10; Abcam), rabbit anti-PCNA (1:20; Abcam), mouse anti-GFAP (1:50, Dako), mouse anti-Nestin (1:100; Abcam), mouse anti–CD133/1 (AC133, 1:11; Miltenyi Biotec), mouse anti–HIF-1α (1:130; Abcam), rabbit anti–HIF-2α (1:130; Abcam), rabbit anti–SOX2 (1:150; Abcam);

each antibody and respective dilution factor was optimized before experimental use. Appropriate controls were used for each staining parameter. After washing, the cells were labeled with the appropriate fluorochrome at 4°C for 15 minutes in the dark. The secondary antibodies used were goat anti–mouse IgG 488 (1:500; Invitrogen), goat anti–mouse IgM 488 (1:500; Invitrogen), goat anti–rabbit IgG 488 (1:500; Invitrogen), goat anti–rabbit IgG 568 (1:500; Invitrogen), goat anti–rabbit IgM 568 (1:500; Invitrogen). After further washing, the labeled cells were analyzed using a BD Biosciences FACSCalibur four-color flow cytometry system (Oxford, United Kingdom), and acquisition and analysis of data were conducted using CellQuest Pro software (BD Biosciences). Propidium iodide (BD Biosciences) allowed the live, positive cell populations to be accurately gated away from necrotic false-positive cells. For the processing of intracellular antigens, the cells were suspended in 100 μl of Cytofix/Cytoperm, a fixation/permeabilization solution (BD Biosciences), for 20 minutes at 4°C before the application of the primary antibody. The flow cytometry technique enabled the analysis of both the percentage mean of the cell population expressing the antigen (percentage-gated expression) and the mean amount of antigen expression by the positive cells, that is, the overall fluorescence level of the total cell population (increase in fluorescence fold intensity).

DNA Preparation and Array Comparative Genomic Hybridization

Genomic DNA was isolated from 1×10^6 cells using a QIAamp DNA mini kit following the manufacturer's instructions (Qiagen Ltd, West Sussex, United Kingdom). DNA copy number analysis was performed using the Agilent Human Genome Microarray Kit 244A (Agilent Technologies Ltd, Santa Clara, CA). Labeling and hybridization were performed according to the manufacturer's instructions (Protocol v1.0 2007; Agilent). Briefly, 2 μg of tumor and sex-matched control genomic DNA (Promega, Southampton, United Kingdom) were differentially labeled with Cy5-dUTP and Cy3-dUTP, respectively, using the Agilent Genomic DNA Kit PLUS (Agilent Technologies Ltd). Labeled products were then column purified. Tumor and control DNA were pooled with 50 mg of human *Cot*I DNA and hybridized to the array with rotation for 40 hours at 65°C. A control array was completed using normal male and female commercially available DNA (Promega). Array washing was performed according to the

Agilent protocol. Each array was scanned using the Innopsys Scanner 700 (Cepheid UK Ltd, Derbyshire, United Kingdom) and analyzed using Imagene and Nexus Copy Number software (BioDiscovery, El Segundo, CA). The array spots that passed all quality thresholds were used for lowness normalization, background corrections, and calculation of $\log_2$ dye ratios. Putative chromosome copy number changes were defined using BioDiscovery's own Rank Segmentation Algorithm, which segments the genome into clusters of uniform $\log_2$ ratios. A significance threshold of $1e - 6$ determined regional segmentation. Threshold cutoffs at ±0.2 and ±0.5 indicated loss or gain of one or two chromosome copies, respectively.

Automated Magnetic Cell Sorting

IN699 cells maintained under hypoxic oxygen tensions were magnetically labeled with CD133/1 (AC133) antibody (Miltenyi Biotec, Bergisch Gladbach, Germany) conjugated to a magnetic microbead in 300 µl of automated magnetic cell sorting running buffer (2 mM EDTA [Sigma-Aldrich], PBS [Sigma-Aldrich], and 0.5% bovine serum albumin [BSA]), 100 µl of FcR blocking reagent (Miltenyi Biotec) and 100 µl of CD133 microbeads (Miltenyi Biotec) at 4°C for 30 minutes in the dark. For magnetic labeling, no more than 1.0×10^8 cells were used. An automated magnetic cell sorting (Miltenyi Biotec) was used for the isolation of CD133; the positive and negative populations were immediately seeded within the appropriate technique and maintained under hypoxic oxygen tension or analyzed by flow cytometry. The purity of the CD133-sorted cells when analyzed by flow cytometry with a FACSCalibur flow cytometry system (Becton Dickinson, Oxford, United Kingdom) was 99% ± 0.316%. The growth kinetics of the CD133⁺ve and CD133⁻ve cell populations were significantly different as identified by 5-bromo-2′-deoxyuridine proliferation analysis, with an increased growth rate observed in the CD133⁺ve cells as identified in Figure 8*B*. With serial passaging, the isolated populations were resegregated to a mixed positive and negative phenotype.

Human Neural Stem Cell Functional Identification

A human NSC functional identification kit (R&D Systems, Ltd, United Kingdom) was used for the short-term maintenance and differentiation of CSCs into neuronal, astrocyte, and oligodendrocyte lineages by using specially formulated differentiation supplements containing insulin-like growth factor and fetal bovine serum. An antibody panel composed of mouse anti–human Nestin, mouse anti–human GFAP, mouse anti–neuron-specific βIII-tubulin, and mouse anti-O4 was used to identify the phenotypes of neural precursors, astrocytes, neurons, and oligodendrocytes.

Oxygen Tension Time Point Analysis

IN699 cells were transferred from atmospheric oxygen (5% CO_2 and atmospheric O_2) to hypoxia (5% CO_2 and 3% O_2). The expression levels of HIF-1α, HIF-2α, and CD133/1 (AC133) were analyzed by flow cytometry with a FACSCalibur flow cytometry system (Becton Dickinson) at the following time points: 0, 24, 48, 72, and 96 hours with relation to the incubation period with hypoxia.

Cell Cycle Analysis

Cells were dissociated and harvested in PBS containing 2 mM EDTA (Sigma-Aldrich), washed once with PBS, and fixed in 70% (vol/vol) ice-cold ethanol for 30 minutes at 4°C. Cells were washed twice with PBS and incubated with 50 mg/ml propidium iodide (Sigma-Aldrich) plus 100 µg/ml RNase (Sigma-Aldrich) for 15 minutes

at RT. Stained nuclei were analyzed with a FACSCalibur flow cytometry system and analyzed using a ModFit 2.0 cell cycle analysis program (Becton Dickinson).

Adhesion Assay

A 96-well plate was coated with 6 µg/ml of fibronectin (Sigma-Aldrich), vitronectin (Sigma-Aldrich), Geltrex (Gibco, Paisley, UK) or 4 µg/ml of BSA (Sigma-Aldrich) in 50 µl/well 1× Tris-buffered saline solution (TBS) and incubated overnight at 37°C. Wells were washed with TBS and blocked with 10 mg/ml of BSA for 30 minutes at RT. After rinsing, 3×10^4 cells/well was added in 100 µl of TBS and incubated at 37°C overnight. After rinsing, cell attachment was quantified with 100 µl/well of substrate/lysis solution (1% Triton X-100, 6 mg/ml *p*-nitrophenylphosphatase [New England Biolabs, Inc, Hertfordshire, United Kingdom] and 50 mM sodium acetate buffer [Sigma-Aldrich]; pH 5.0), incubated at 37°C for 90 minutes. The reaction was quenched with 50 µl/well of 1 M NaOH and immediately read on a FLUOstar OPTIMA plate reader (BMG LABTECH, Ortenberg, Germany) with a 405-nm filter.

Proliferation Assay

A colorimetric immunoassay kit (Roche Diagnostics, Mannheim, Germany) was used for the quantification of cellular proliferation based on the measurement of 5-bromo-2′-deoxyuridine incorporated during DNA synthesis. To analyze the proliferation indices (PIs) in the presence of extracellular matrices (ECMs), the 96-well plate was coated with 6 µg/ml of fibronectin, vitronectin, Geltrex, or 4 µg/ml of BSA (in 50 µl/well of 1× TBS) and incubated overnight at 37°C before PI immunoassay according to the manufacturer's instructions.

Invasion Assay

For the invasion assay, 6.0 µg/ml of Geltrex, vitronectin, or fibronectin (in 50 µl of TBS, incubated overnight at RT) was coated to the upper compartment of 8.0-µm pore Transwell inserts (Corning Costar, New York, NY). A total of 1×10^6 cells/ml were added to the upper "Costar" compartment (after 24 hours of starvation of medium supplements). To the lower compartment, 650 µl of NBM supplemented with 10 µg/ml platelet-derived growth factor (PDGF-AB) (Miltenyi Biotec, UK) was added and incubated at 37°C for 5 hours. The hematologic stain, Diff-quick (Bio-Rad, Hertfordshire, United Kingdom) was used to assay the invaded cells on the basal layer of the Transwell insert. The mean number of invasive cells was quantified using an Olympus IX71 research inverted system microscope (Olympus, Essex, United Kingdom).

Statistical Analysis

Student's *t* test was used for statistical evaluation ($P < .005$). All data presented are representative of three independent experiments performed in triplicate ($n = 3$). All values are shown as arithmetic means ± standard errors of the mean (SEM).

Results

CD133⁺ve and CD133⁻ve Cell Fractions Display Similar Stemness and Differentiation Capacities

To confirm the presence of stem cells and the capacity for multilineage differentiation, qualitative and quantitative immunofluorescence was performed. Sox-2, Nestin, Olig-2, and Musashi-1 are frequently

used as markers for an undifferentiated state. Analyzing Sox-2 expression by flow cytometry, we detected 93.5% ± 1.425% Sox-2$^+$ve cells in the CD133$^+$ve cell fraction. Similarly, CD133$^-$ve cells displayed 92.34% ± 1.44% Sox-2$^+$ve cells. Using fluorescence immunocytochemistry, strong Sox-2 levels were also identified in both cell fractions. By flow cytometry, the CD133$^+$ve and CD133$^-$ve cell fractions were 95.3% ± 0.45% and 95.4% ± 0.523% Olig-2$^+$ve, respectively. Olig-2 positivity was also detected with fluorescence immunocytochemistry localized within the cytoplasm. Nestin expression was restricted to the cell bodies of both cell fractions. By flow cytometry, we detected 90.4% ± 0.551% Nestin$^+$ve cells in the CD133$^+$ve fraction and 81.7% ± 1.21% Nestin$^+$ve cells in the CD133$^-$ve cell fraction. We also identified Musashi-1$^+$ve cells typically localized to the cytoplasm of CD133$^+$ve and CD133$^-$ve cells. Flow cytometry detected 96.9% ± 0.205% Musashi-1$^+$ve cells in the CD133$^+$ve fraction and 87.4% ± 3.58% positivity in the CD133$^-$ve fraction. Although both fractions displayed stemness, the CD133$^-$ve fraction displayed statistically significant decreased expression with Nestin and Musashi-1 but not with Olig-2 and Sox-2.

We next evaluated the multipotency of CD133$^+$ve and CD133$^-$ve cell fractions by inducing differentiation and expansion into neuronal, astrocytic, and oligodendrocytic lineages. After 3 days of expansion, fluorescent immunocytochemistry showed immunoreactivity for GFAP (astrocytes), βIII-tubulin (neurons), and Olig-4 (oligodendrocytes) in both cell fractions. Stemness and differentiation analysis are summarized in Figures 2 and 3.

CD133/1 Expression under Atmospheric and Hypoxic Oxygen Conditions in IN699

The expression of CD133 in the IN699 cells cultured under atmospheric and hypoxic culture conditions was assessed by flow cytometry. The percentage of the cell population expressing CD133 as well as the fluorescence fold expression under atmospheric and hypoxic culture conditions assessed by flow cytometry is shown in Figure 4. Hypoxia caused a significant increase in the levels of CD133 plus a 30-fold increase in CD133 expression (expressed as fluorescence fold change) in comparison to the IN699 cells cultured under atmospheric growth conditions. The cellular location of CD133 and the expression level patterns under hypoxic and atmospheric oxygen conditions were further confirmed by fluorescence immunocytochemistry as shown in Figure 5. The cellular location of CD133 was typically identified as spanning the plasma membrane under both oxygen tensions with a significant increase in CD133 expression with hypoxia.

DNA Copy Number Analysis in IN699 Parental, CD133$^+$ve, and CD133$^-$ve Cell Populations

Genomic copy number profiles generated for IN699 parental cells and for the CD133$^+$ve and CD133$^-$ve fractions were essentially identical, allowing for interarray variation (Figure 6). All of the three cell populations displayed multiple copy number aberrations involving all chromosomes and indicating a complex tumor karyotype. With the exception of monosomy 4, all autosomes demonstrated interstitial
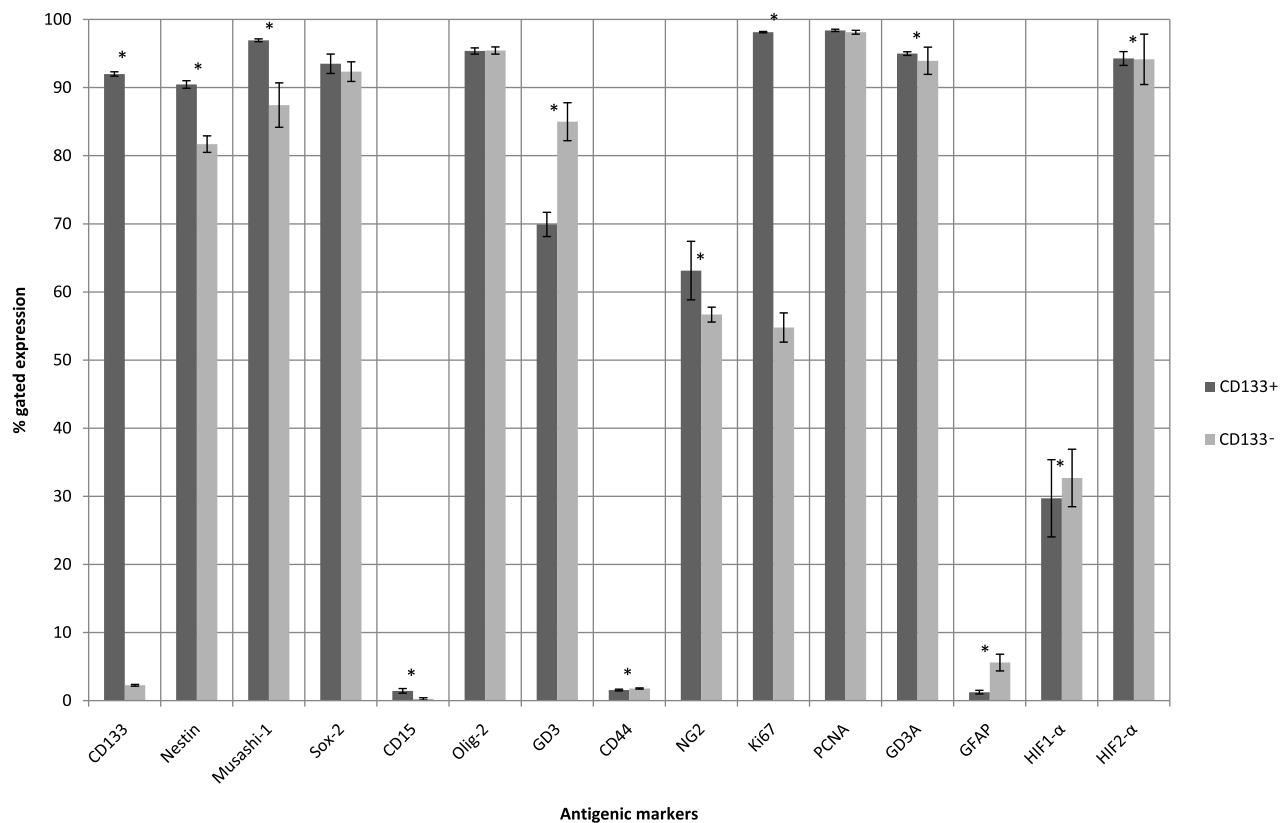
Figure 2. The percentage mean (percentage-gated expression) of cells displaying positivity for each antigen for the CD133$^+$ve (blue) and CD133$^-$ve (red) cell fractions, cultured under hypoxia (3% O$_2$ and 5% CO$_2$), analyzed by flow cytometry. Student's *t* test was used for statistical evaluation (*$P < .005$). All data presented are representative of three independent experiments performed in triplicate ($n = 3$). All values are shown as arithmetic means ± standard errors of the mean.
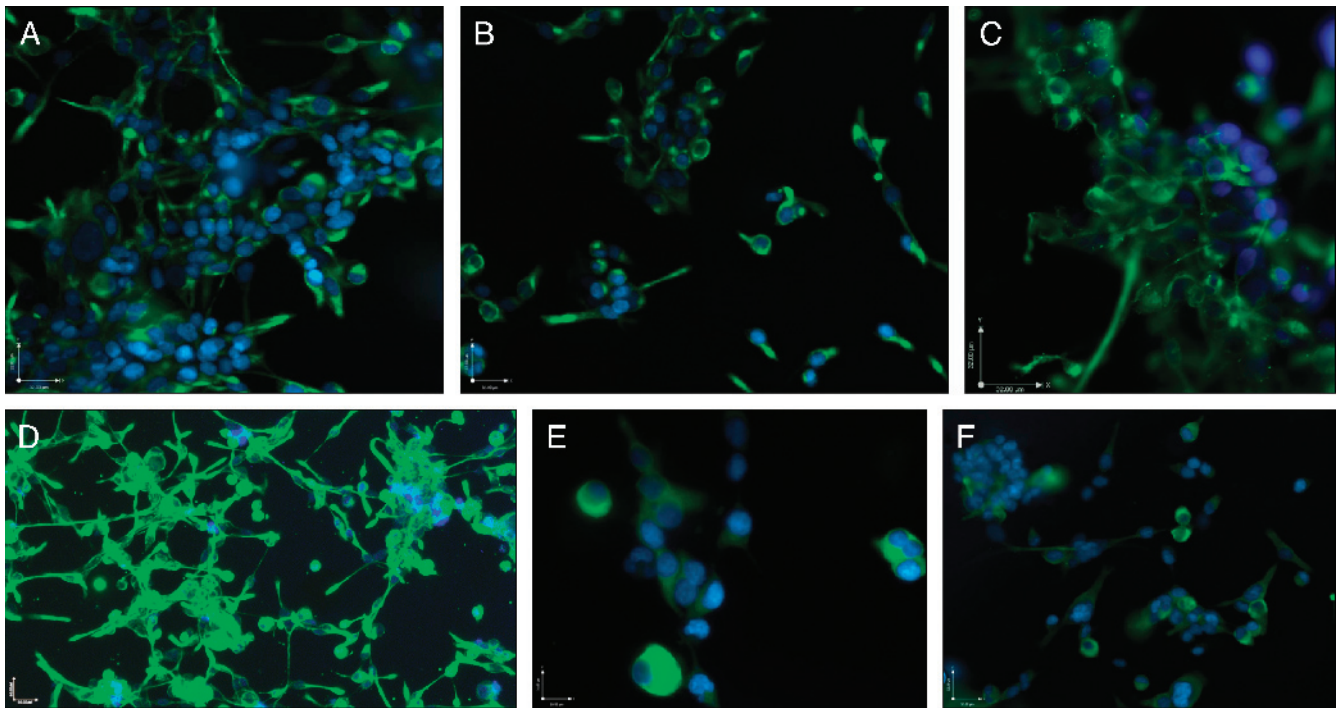
Figure 3. Fluorescence immunocytochemistry of isolated CD133$^+$ve and CD133$^-$ve cells characterized with stem cell markers and markers of multilineage differentiation. The cellular location of Nestin seems to be within the cytosol and cellular processes of both isolated cell cultures (A and B). GFAP was highly expressed in both cell types, localized within the cytoplasm and cellular processes (C and D). Fluorescence staining for Olig-4 (E and F) was also observed within both cell cultures, primarily located around the periphery of the nucleus. Staining for stemness and multilineage differentiation are shown in green (AlexaFluor 488) and counterstained with Hoescht blue.

regions of either homozygous loss, loss, gain, and/or high copy gain. A summary of gains and losses is given in Table W1, including cytoband locations and sizes of aberrations.

Expression Levels of the CD133 Glycoprotein Are Inversely Proportional to HIF-1α

HIF-1α and HIF-2α are essential transcription factors moderating changes in gene expression in response to hypoxia. HIF-1α, HIF-2α, and CD133 antigen and glycoprotein levels were determined in the parental cell culture with decreasing oxygen tension during a 96-hour period. The percentage mean of the HIF-2α antigen remained significantly ($P < .005$) elevated, with decreasing oxygen with positivity ranging from 98.0% ± 0.24% to 99.4% ± 0.135%. In contrast, HIF-1α positivity rapidly declined from 76.7% ± 5.5% to 2.7% ± 0.38%. On the analysis of antigen expression (fluorescence fold expression), a positive correlation between HIF-2α and CD133 was observed with decreasing oxygen tension ($P < .005$) displaying a cumulative increase between HIF-2α and CD133. In contrast, an inversely proportional relationship between CD133 and HIF-1α was seen ($P < .005$); as the levels of CD133 increased with hypoxia, the levels HIF-1α decreased. It is clear that a relationship between HIF-2α and CD133 exists, which may be implicated in the regulation of the stem cell phenotype with decreasing oxygen tension. Decreasing oxygen tension effects HIF-1α but is not mirrored by HIF-2α in IN699. The expression levels of HIF-2α were seen to be independent of oxygen tension and culture conditions. The relationship between CD133 and HIF-1α and HIF-2α respectively are summarized in Figure 7.

Cell Cycle and Proliferation Analysis of IN699 and CD133$^+$ve and CD133$^-$ve Cell Fractions Derived Therefrom

On comparison of both oxygen tensions, the G_1 phase represented most of the cycling cell population. Under atmospheric conditions, the G_1 phase represented 81% ± 0.328% of the cell population. However, with decreasing oxygen tension, the percentage of active cells within the G_1 phase decreased to 71% ± 0.88%. The S phase and G_2/M phases of each tension were virtually equal; with increased oxygen tension, the cycling cells in the S phase and the G_2/M phase are 8.6% ± 0.322% and 9.4% ± 0.026%, respectively, and with reduced oxygen, the S phase and the G_2/M phase cell population numbers increased to 13.7% ± 0.12% and 14% ± 0.85%, respectively. For both the CD133$^+$ve and CD133$^-$ve cell fractions, the G_1 phase represented most of the actively cycling cell populations, displaying values of 82.32% ± 1.46% and 78.73% ± 1.43%, respectively. The percentages of cycling cells for both cell populations within S and G_2/M phases were virtually equal. The S and G_2/M phases for the CD133$^+$ve fraction displayed 8.0867% ± 1.069% and 9.15% ± 0.35%, respectively. The S and G_2/M phases for the CD133$^-$ve cell fractions were 8.92% ± 0.73% and 10.71% ± 0.19%, respectively. The proportion of actively cycling cells within the S phase differed between the two oxygen tensions. Under atmospheric growth conditions, we observed the PI to be 0.148 ± 0.0074; this value increased to 0.168 ± 0.016 with decreasing oxygen tension. These PIs confirm the results of the cell cycle analysis; the proportion of the S-phase parental cells with decreased tension surpasses those with increased oxygen tensions, implicating hypoxia or HIFs in the modification of proliferation (Figure 8, A and B). The proportion of actively cycling
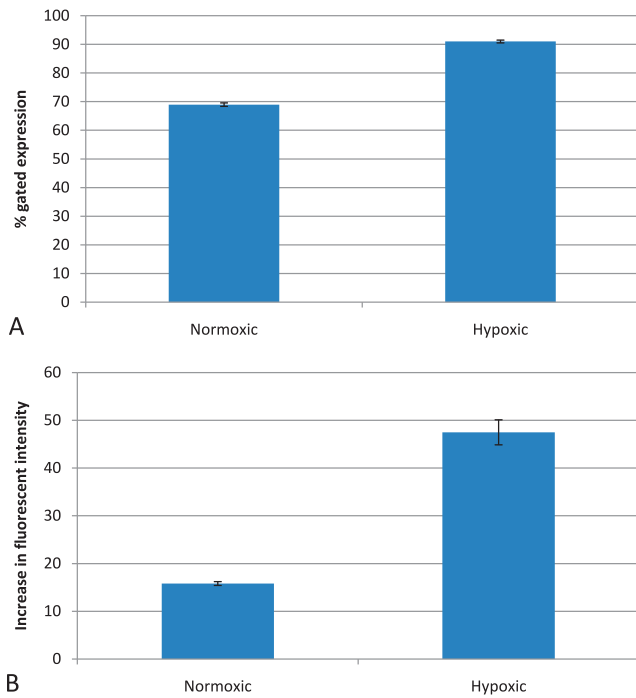
Figure 4. (A) Percentage mean (percentage-gated expression) of the parental IN699 cells displaying positivity for the CD133 antigen under atmospheric and hypoxic oxygen tensions as analyzed by flow cytometry. (B) Mean amount of CD133 antigen expression as shown by an increase in fluorescence fold intensity (i.e., overall fluorescence level of the total cell population) in the parental pediatric GB cell culture (IN699) under atmospheric and hypoxic culture conditions as analyzed by flow cytometry. Student's t test was used for statistical evaluation ($P < .005$). All data presented are representative of three independent experiments performed in triplicate ($n = 3$). All values are shown as arithmetic means ± standard errors of the mean.

cells within the S phase differed between the two cell fractions. These PIs correlate with the results of the cell cycle analysis because there was only a marginal disparity between the CD133^{+}ve and CD133^{-}ve cells with regard to the S phase of the cell cycles. We observed a PI of 0.111 ± 0.00715 with regard to the CD133^{+}ve fraction and 0.098 ± 0.00408 for the CD133^{-}ve cells (data not shown). The PI of the parental culture showed substantial differences when cultured in the presence of varying ECMs and oxygen tensions (Figure 8, A and B). Vitronectin induced the greatest proliferation modifications. Under atmospheric conditions, the index was observed at 0.193 ± 0.0132; however, with decreasing oxygen tension, the index decreased to 0.130 ± 0.00165. Similarly, fibronectin also induced a PI of 0.130 ± 0.00346 with normoxia. However, with decreasing oxygen tension, the PI was observed at 0.181 ± 0.056. Although Geltrex induced the least-variant modifications between oxygen tensions, this ECM stimulated the highest index with hypoxia (0.141 ± 0.00385). These results indicate that cell proliferation increases with increasing oxygen tensions in the presence of ECMs, suggesting that cell adhesion upregulates DNA synthesis. The CD133^{+}ve population displayed the highest PI values for each ECM in comparison to the CD133^{-}ve fraction (Figure 8). Of the ECMs investigated, BSA (the control sample) instigated the highest PI at 0.195 ± 0.00465, followed by Geltrex at 0.161 ± 0.0098. Vitronectin and fibronectin induced an almost identical PI response at 0.109 ± 0.00524 and 0.104 ±

0.00507, respectively. Similarly, the highest PI for the CD133^{-}ve fraction was also induced with BSA (control) at 0.161 ± 0.00458 (17% less than the CD133^{+}ve fraction, $P < .005$), followed by Geltrex at 0.144 ± 0.0045 (10% less than the CD133^{+}ve fraction, $P > .005$). The PI for vitronectin decreased by 0.01 ± 0.00049 for the CD133^{-}ve cells, in comparison to the CD133^{+}ve fraction, and in a similar response to the CD133^{+}ve cells, fibronectin resulted in the least significant ECM at 0.00872 ± 0.004.

Propensity of Cell Attachment Increases with Normoxia

An increased propensity of cell attachment was observed with increasing normoxia. Of the ECMs investigated, fibronectin produced the highest attachment rate at 1.604 ± 0.025, followed by vitronectin (1.584 ± 0.038) and BSA (0.987 ± 0.06). The lowest cell adhesion rate was produced with Geltrex (0.626 ± 0.017). Cell attachment rates decreased significantly with decreasing oxygen tension. Of the ECM proteins investigated with hypoxia, vitronectin produced the highest adhesion rate (0.645 ± 0.035, $P < .005$), followed by fibronectin (0.615 ± 0.015, $P < .005$) and BSA (0.504 ± 0.016,

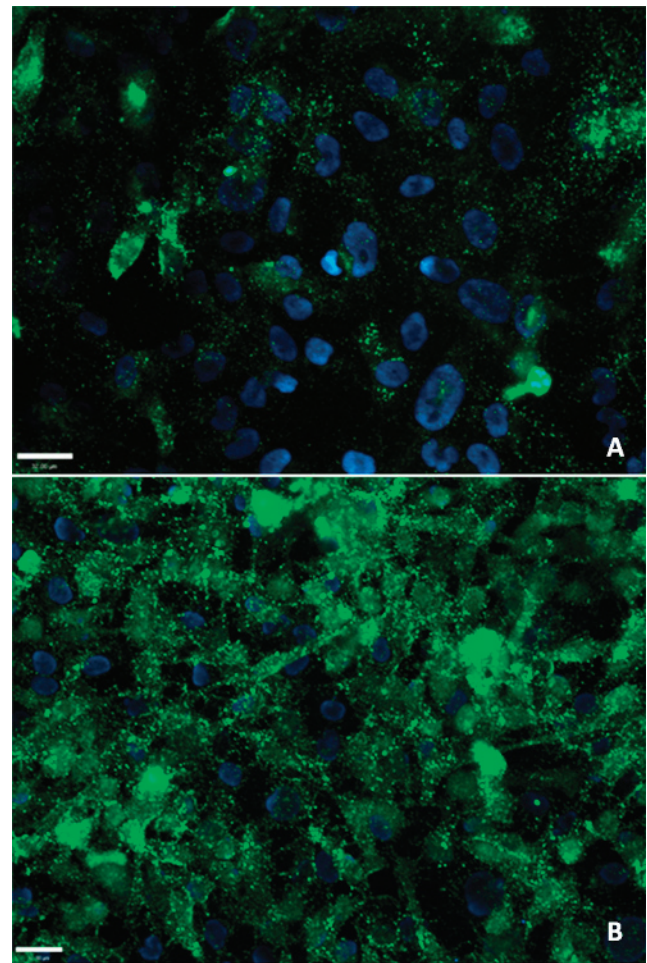**Figure 5.** Characterization of the parental pediatric GB cell culture (IN699) with CD133 (green) and counterstained with Hoescht blue under atmospheric (A) and hypoxic (B) oxygen tensions with fluorescent immunocytochemistry. The cellular location of CD133 was typically identified as spanning the plasma membrane under both oxygen tensions with a significant increase in CD133 expression with hypoxia. Scale bar, 32 μm.
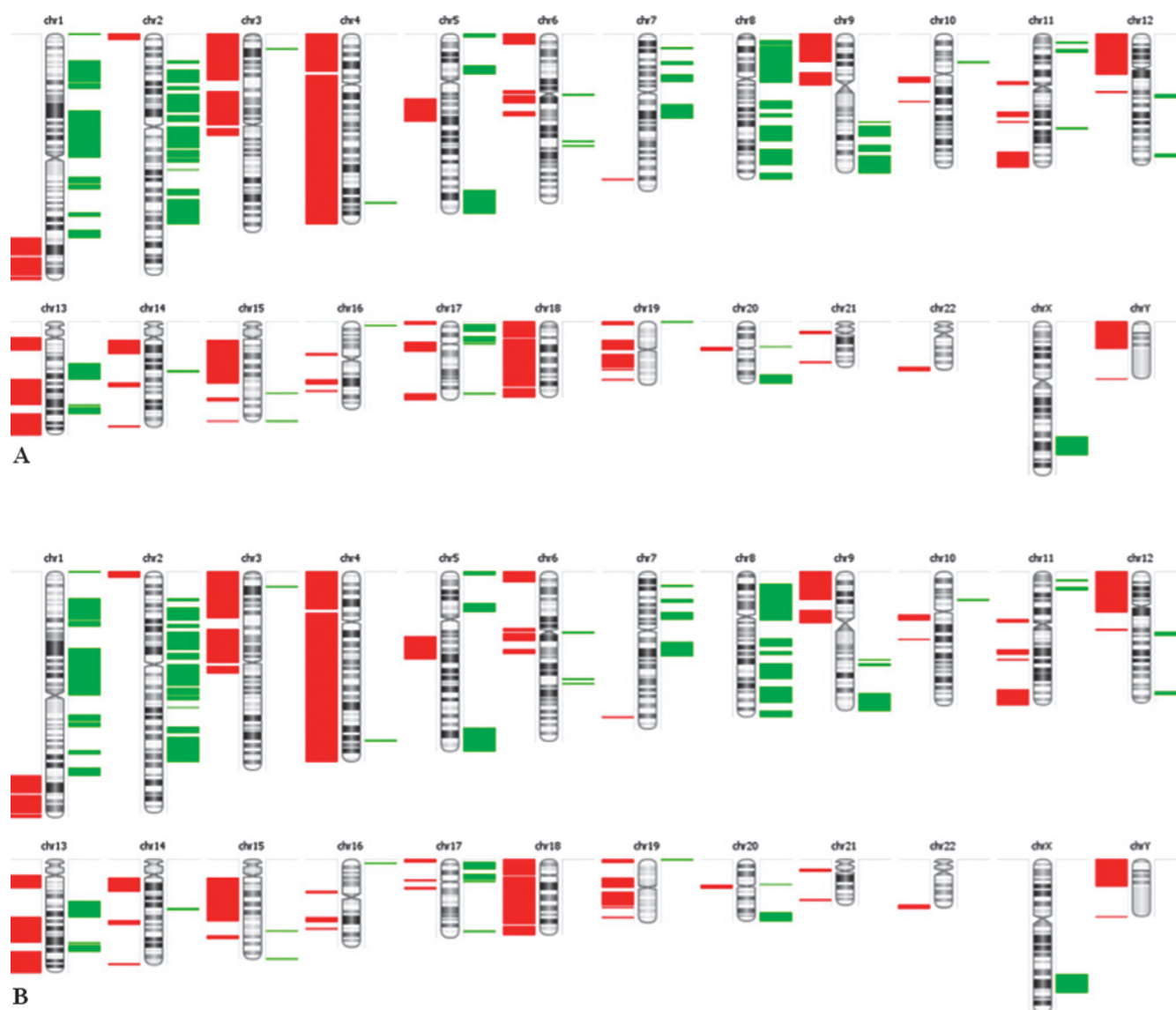
Figure 6. An overview of the DNA copy number alterations in IN699 for (A) CD133⁺ve and (B) CD133⁻ve cell fractions. Green blocks indicate regions of chromosome gain and red blocks regions of loss.

$P < .005$). Again, the lowest cell adhesion rate was induced with Geltrex (0.389 ± 0.021, $P < .005$). The propensity of cell attachment is summarized in Figure 8. Quantification of the CD133⁺ve and CD133⁻ve cell adhesion assays demonstrated an overall 6% elevated propensity for cell adhesion within the CD133⁻ve cell fraction for each ECM investigated, in comparison to the CD133⁺ve population. Of the ECMs assayed, Geltrex induced the highest rate of attachment for the CD133⁻ve population at 0.396 ± 0.00686, followed by vitronectin at 0.377 ± 0.1 and BSA at 0.366 ± 0.017. The least instigative adhesive ECM was fibronectin (0.355 ± 0.0196). Adhesion analysis of the CD133⁺ve fraction also showed Geltrex to instigate the highest level of adhesion at 0.3856 ± 0.009, followed by vitronectin at 0.356 ± 0.058 and BSA at 0.347 ± 0.0786. Again, the lowest cell adhesion was observed by fibronectin at 0.323 ± 0.0073. Quantification of CD133 adhesion propensities is summarized in Figure 8. Analyzing CD44 expression by flow cytometry, we detected $1.201\% \pm 0.135\%$ CD44⁺ cells in the CD133⁺ve cell fraction and $1.503\% \pm 0.073\%$ CD44⁺ cells in the CD133⁻ve cell fraction (Figure 8).

Hypoxia Increases the Invasive Propensity of IN699 Cells

Invasion propensity (I_P — the innate propensity of cells to invade) levels correlated with decreasing oxygen tension in the parental cell culture. The ECM Geltrex produced the highest I_P with a value of 40.4 ± 4.85, an increase of 73% than that observed under atmospheric growth conditions (10.6 ± 3.09). With decreasing oxygen tensions, fibronectin induced an I_P of 18.6 ± 1.066, a 62% increase than that observed with normoxia (7.067 ± 1.6). Although vitronectin instigated the lowest I_P of both oxygen tensions, the I_P with increasing oxygen tensions (5.213 ± 1.235) was 63.32% less than that noted with hypoxia (14.21 ± 1.645; Figure 8).

CD133⁻ve Cells Show Greater Invasion Propensity than CD133⁺ve Cells

The CD133⁻ve cell fraction possessed the most significant I_P ($P < .005$) for each ECM investigated, supporting the notion of a possible positive correlation between adhesion and invasion. The highest CD133⁻ve cell I_P was observed with vitronectin at 84 ± 12, 74%
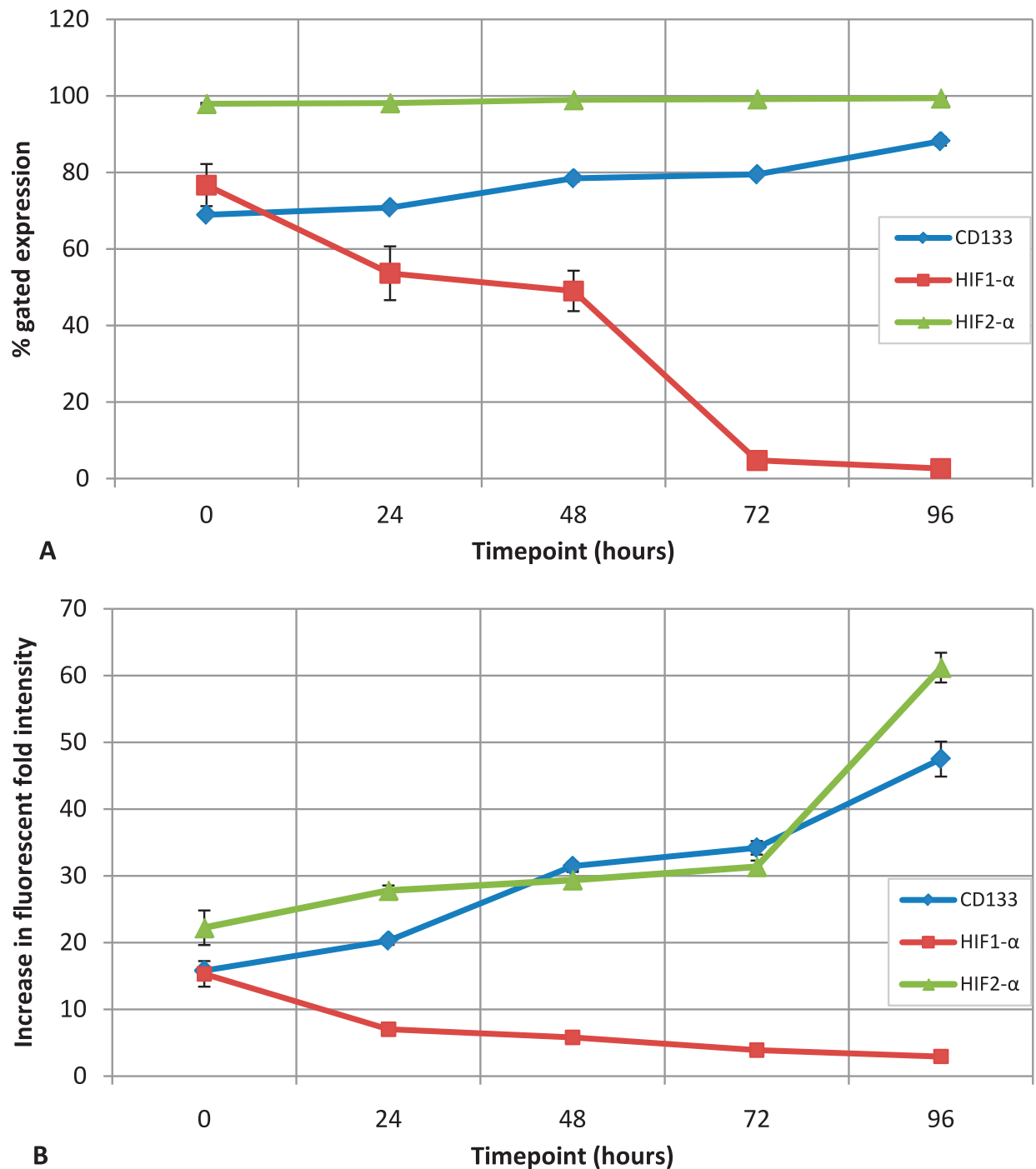
Figure 7. (A) Percentage mean (percentage-gated expression) of the parental pediatric GB cell culture (IN699) expressing the antigens CD133, HIF-1α, and HIF-2α at the following time points: 0, 24, 48, 72, and 96 hours with relation to the incubation period with hypoxia. Although the levels of HIF-2α remain constant with hypoxia, the levels of HIF-1α seem to be inversely proportional to decreasing oxygen tension. A positive correlation between decreasing oxygen tension and CD133 is also apparent. Student's *t* test was used for statistical evaluation ($P < .005$). All data presented are representative of three independent experiments performed in triplicate ($n = 3$). All values are shown as arithmetic means ± standard errors of the mean. (B) Mean amount of CD133, HIF-1α, and HIF-2α antigen expression as shown by an increase in fluorescence fold intensity (i.e., overall fluorescence level of the total cell population) in the parental pediatric GB cell culture (IN699) at the following time points: 0, 24, 48, 72, and 96 hours with relation to the incubation period with hypoxia. A positive correlation between HIF-2α and CD133 was observed with decreasing oxygen tension. However, in contrast, an inversely proportional relationship between CD133 and HIF-1α with decreasing oxygen tension can be seen. Student's *t* test was used for statistical evaluation ($P < .005$). All data presented are representative of three independent experiments performed in triplicate ($n = 3$). All values are shown as arithmetic means ± standard errors of the mean.
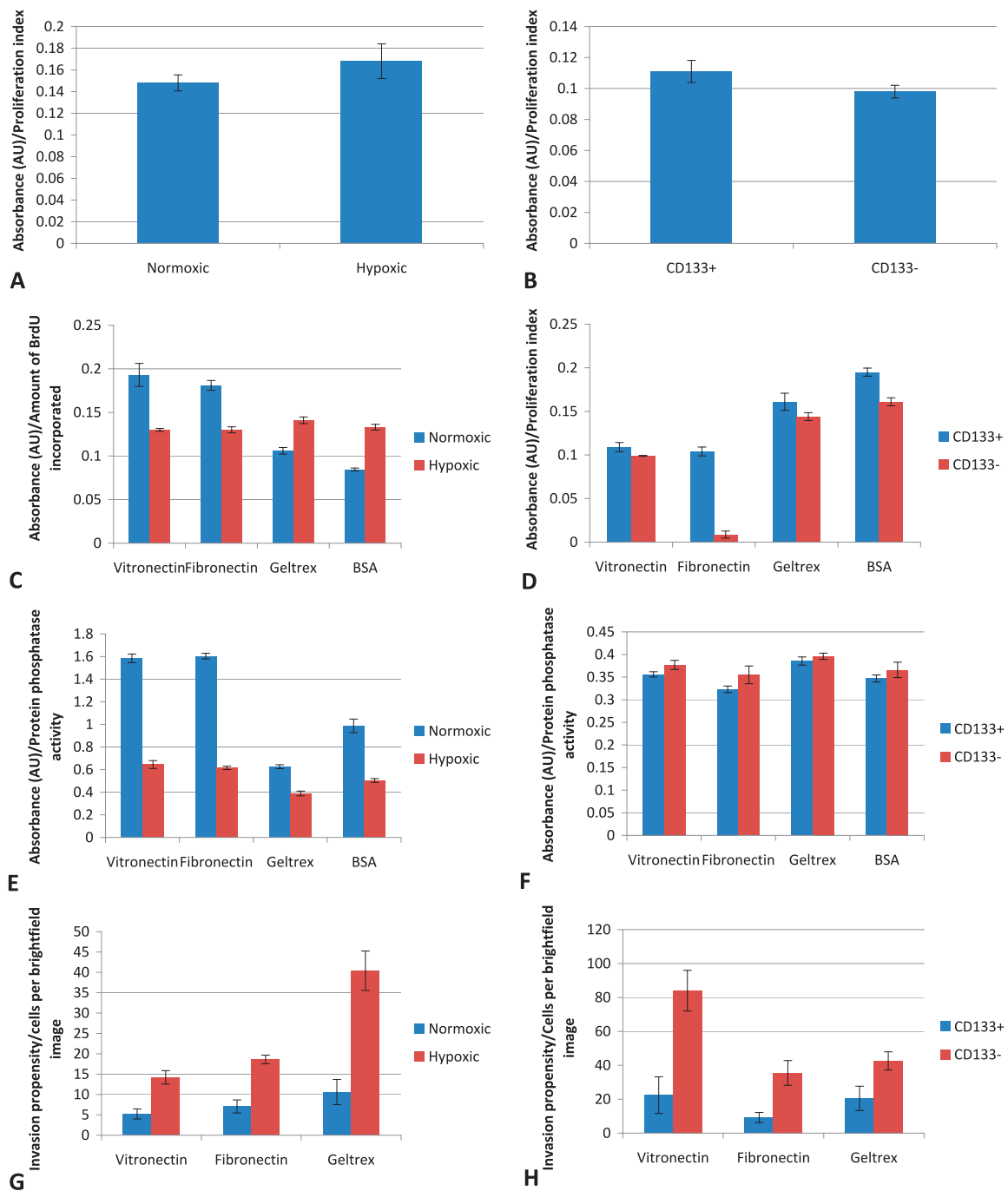
Figure 8. (A) PI analysis of the parental pediatric GB cell culture (IN699) with BrdU under atmospheric and hypoxic growth conditions. (B) PI analysis of CD133^{+}ve and CD133^{−}ve cells with BrdU with hypoxia. (C) Cell attachment propensity analysis of the parental pediatric GB cell culture (IN699) under atmospheric and hypoxic oxygen tensions, cultured in the presence of vitronectin, fibronectin, Geltrex, and BSA (control sample). (D) Cell attachment propensity analysis of CD133^{+}ve and CD133^{−}ve cell fractions, cultured in the presence of vitronectin, fibronectin, Geltrex, and BSA (control sample) under hypoxic oxygen tension. (E) Invasion propensity analysis of the parental pediatric GB cell culture (IN699) under atmospheric and hypoxic oxygen tensions, cultured in the presence of vitronectin, fibronectin, and Geltrex. (F) Invasion propensity analysis of isolated CD133^{+}ve and CD133^{−}ve cell fractions, cultured in the presence of vitronectin, fibronectin, and Geltrex with decreasing oxygen tensions. (G) PI analysis of the parental pediatric GB cell culture (IN699) under atmospheric and hypoxic oxygen tensions, cultured in the presence of vitronectin, fibronectin, Geltrex, and BSA (control sample). (H) PI analysis of isolated CD133^{+}ve and CD133^{−}ve cell fractions, cultured in the presence of vitronectin, fibronectin, Geltrex, and BSA (control sample) with decreasing oxygen tension. All data presented in Figure 7 are representative of three independent experiments performed in triplicate ($n = 3$). All values are shown as arithmetic means ± standard errors of the mean. Student's t test was used for statistical evaluation ($P < .005$).

more invasive than the CD133$^+$ve cells with vitronectin (22.4 ± 10.8). The CD133$^-$ve cells were seen to be 75% more invasive than the CD133$^+$ve cells when assayed with fibronectin (35.5 ± 7.3 and 9.2 ± 2.96, respectively) and 52% more invasive when assayed with Geltrex (42.56 ± 5.369 and 20.5 ± 7.17, respectively). Analyzing GD3 and acetylated GD3 expression by flow cytometry, we detected 4.225% ± 0.61% GD3$^+$ cells and 15.04% ± 0.073% GD3$^A{}^+$ cells in the CD133$^+$ve cell fraction and 4.48% ± 1.09% GD3$^+$ cells and 24.86% ± 4.3% GD3$^A{}^+$ cells in the CD133$^-$ve fraction (Figure 8).

Discussion

The role of CD133 as a CSC marker is both enigmatic and controversial. Any evidence pointing toward a specific functional role of CD133 may be significant in determining whether CD133 may be appropriate as a CSC or "tumor-initiating cell" marker. Moreover, CD133 has not yet been correlated to a contributing role in "cancer stemness" [21] owing to the lack of knowledge surrounding the glycoprotein. To determine a possible link between CD133 expression and biologic function, the biologic behavior of CD133$^+$ve and CD133$^-$ve cells with different oxygen tensions must be ascertained. Using a pediatric GB containing unprecedentedly high levels of CD133$^+$ve cells as a study model, we have attempted to correlate CD133 expression with cellular phenotype and biologic behavior.

Brain tumor stem cells (BTSCs) are characterized by 1) the ability to self-renew, 2) the capacity to initiate brain tumors, and 3) the ability to differentiate into cells of neuronal, astrocytic, and oligodendroglial lineage [22,23]. After isolation, CD133$^+$ve cells were observed to coexpress (to a very high degree) Musashi-1, Nestin, Olig-2, and Sox-2. Musashi-1, a cytoplasmic antigenic marker of early development, indicates a neural origin [24]. Therefore, CD133$^+$/Musashi-1$^+$ BTSCs resemble the phenotype of NSCs during early cortical development [25]. This finding is supported by the coexpression of CD133 and Musashi-1, indicating an NSC characteristic of CD133$^+$ve cells [26]. Moreover, Musashi-1 expression is of functional significance for preserving self-renewal and multipotency in stem cells [27]. GB cells that express high levels of Musashi-1 display significantly higher levels of Notch-1 in comparison to cells with less Musashi-1 [28]. Hyperactivation of Notch-1, through Musashi-1, results in tumorigenesis and the maintenance of an immature phenotype [27], which may begin to explain the elevated PI observed in the CD133$^+$ve cells, in comparison to the CD133$^-$ve cells.

In the present study, the CD133$^+$ve cells indicated a neural origin, established by the CD133$^+$/Nestin$^+$ phenotype, because Nestin is produced by NSCs in the mammalian CNS during development to preserve the rapid self-renewal of NSCs [29]. Moreover, downregulation of the Nestin protein is associated with NSC differentiation [30]. The production of Nestin by NSCs also makes this antigen a marker of proliferation because it is associated with the hyperactivation of N-*myc* [31]. In the present study, the IN699 CD133$^+$ve cells displayed upregulated expression of Nestin in comparison to the CD133$^-$ve cell fraction, which may account for the marked difference in PIs between the two populations.

During early embryonic CNS development, the basic helix-loop-helix transcriptional repressor protein, Olig-2, plays a pivotal role in maintaining NSCs and progenitor cells in a state of continuous replication. Of the IN699 CD133$^+$ve and CD133$^-$ve cell fractions, almost all cells (approximately 95%) were positive for Olig-2. Similar findings have been previously reported, demonstrating 98% of GB

CD133$^+$ve cells to be positive for Olig-2 [32]. Many research groups have shown that all high-grade malignant gliomas, independent of histologic type, contain Olig-2$^+$ve cells [32–36]. The expression pattern of Olig-2 is therefore not conserved to a particular subset of cells, explaining the IN699 CD133$^+$/Olig2$^+$ and IN699 CD133$^-$/Olig2$^+$ phenotypes observed, indicating neuronal and oligodendroglial lineages [32,35]. The presence of Olig-2 may be of significance to "stemness" because it has been directly linked to cyclin-dependent kinases implicated in the control of the p21 gene [37]. The repression of p21 by Olig-2 results in the up-regulation of DNA synthesis, increasing the levels of PCNA [37] correlating with the high expression levels of PCNA observed in both the IN699 CD133$^+$ve and CD133$^-$ve cells, 98.4% and 98.1%, respectively.

Sox-2 is associated with the development of NSCs within the CNS; therefore, CD133$^+$/Sox-2$^+$ BTSCs may resemble the phenotype of NSCs [38]. The transcription factor Sox-2 serves a functional role in sustaining the growth and renewal of NSCs. Silencing of Sox-2 in GB cells has been shown to attenuate the expression of Ki67, implicating Sox-2 with cell cycle control [38], thus supporting our observed correlation of Sox-2 and Ki67 expression in CD133$^+$ve cells, maintaining rapid cell cycle turnover and upregulated proliferation rates. Sox-2 expression has been documented in many malignant tissues [39–44]. In addition, Sox-2 was identified not only to be expressed in NSCs but also in early progenitor cells [38]. Because the IN699 cells were cultured in NBM, optimized to support and maintain the growth of stem and transiently dividing progenitor cells, this may explain why Sox-2 is present in the IN699 CD133$^-$ve fraction. Therefore, instead of indicating "stemness," Sox-2 may be indicative of early progenitors. This finding correlates with the decreased expression levels of Ki67 observed in the IN699 CD133$^-$ve cells. A similar expression pattern of Sox-2 and Ki67 has been reported in CD133$^+$ve and CD133$^-$ve GBM cells when cultured under NSC-specific cell culture conditions [45]. Moreover, the expression of Sox-2 may decrease rapidly in cells maintained under differentiating conditions [38], further supporting the notion that the IN699 CD133$^-$ve cells are early progenitor cells.

The stage-specific embryonic antigen (SSEA-1/LEX)/CD15 is said to positively identify tumor stem cells or tumor–initiating cells in human GBs [46]. However, in the present study, the isolated CD133$^+$ve and CD133$^-$ve cell fractions displayed little expression (approximately 1%) for CD15, raising the possibility that CD15 may not be a universally enriched antigenic marker for BTSCs. CD15 has been implicated in the metastatic spread of cancer cells by functioning in both homophilic binding and as a ligand for P-selectin and E-selectin on vascular endothelium [47]. The absence of the CD15 antigen in the IN699 CD133$^+$ve and CD133$^-$ve cell fractions is consistent with the previous explanation for the general failure of intrinsic human brain tumors to metastasize, by preventing the adhesion of neoplastic glia to "target" organ endothelium outside the CNS [48].

The lineage commitment and differentiation stages of gliomas are unclear [48]. Although it is uncommon for a single glioma to exhibit the entire range of cell types generated by a NSC, gliomas are often composed of multiple cell types such as astrocytes and oligodendrocytes [49]. In the present study, pluripotency was confirmed by the expression of βIII-tubulin (neuronal), GFAP (astrocytic), and O4 (oligodendrocytic) lineage markers. These findings are consistent with the research conducted by Beier et al.; a sphere derived from a single CD133$^+$ve cell displayed positivity for the three neural lineages, contributing a link to the cancer "stemness" connected to the

glycoprotein [16]. However, whether CSC-derived differentiated neoplastic cells can actually fulfill neural functions has yet to be addressed. Isolated IN699 CD133⁻ve cells were also observed to exhibit neural lineage. These observations suggest that the heterogeneity within gliomas may be a result not only of the NSC but also of the neural progenitor cells [49]. If correct, this would explain the presence of mixed cell gliomas, arising from the transformation of a single bipotential cell [49,50], plus the blocked differentiation phenomenon [51]. Progenitor cells, activated with GB signal transduction proteins Akt and kRas, have also been reported to give rise to brain tumors in rodents with histologically similar characteristics to GBs [52]. Alternatively, the expression of the lineage-specific marker may not be a result of cell type; instead, it may indicate the differentiation stage(s) characteristic of glioma cells and the normal glial genesis hierarchy.

Local oxygen concentrations can also directly influence stem cell self-renewal. An attractive notion is that stem cells, particularly in long-lived animals, benefit from residing in hypoxic niches where oxidative DNA damage may be reduced [13]. In the present study, CD133 expression increased with decreasing oxygen tension. Furthermore, the percentage-gated expression of CD133 antigens was observed to positively correlate with the increasing numbers of HIF-2α. Recent reports have identified molecular mechanisms whereby HIFs directly modify cellular differentiation and stem cell functions. Therefore, a relationship between HIF-2α and CD133 must exist and is implicated in the regulation of the stem cell phenotype. In the present study, HIF-2α was seen to increase under hypoxic conditions along with increasing CD133 expression. Thus, HIF-2α may regulate CD133 expression, whereas HIF-1α, which decreased under 3% oxygen conditions, seems to counterbalance CD133 regulation. Moreover, hypoxia has been shown to block NSC differentiation in a Notch-dependent manner [53]; furthermore, HIF-2α promotes c-Myc transcriptional activity, further stabilizing an immature cell state [54]. Indeed, HIF-1α has been shown to antagonize c-Myc transcriptional activity under hypoxia, resulting in the up-regulation of $p21$ and cell cycle arrest, whereas HIF-2α promotes c-Myc function, through cyclin D2, inducing cell cycle progression [55], which may explain the down-regulation of HIF-1α observed with increasing levels of CD133 and HIF-2α.

Although hypoxia induced a high invasive propensity of the parental IN699 culture and the CD133⁻ve cells, cellular adhesion (i.e., the number of cells attached) was decreased. Quantification of cell attachment demonstrated that, although the CD133⁻ve cells were observed to increase in number of cells attached with all of the ECMs analyzed (significantly vitronectin and fibronectin), in relation to the IN699 CD133⁺ve cells, the number of cells attached was not significant. These findings suggest that the CD133 glycoprotein does not act as an adhesion molecule. In contrast, the microenvironment does seem to exert a significant influence on cellular adhesion, with the number of attachments significantly decreasing with hypoxia. Quantitative cell analysis of the IN699 parental culture showed a significant decrease in cellular attachment to vitronectin and fibronectin under hypoxia. In concert with this adhesion to vitronectin and fibronectin by MDA-MB-231, breast cancer cells were reduced with hypoxia and little difference in the adhesiveness of these cells to either substrate was also noted [56]. It therefore seems that decreasing oxygen tension induces a decline in cellular adhesion. It is well recognized that cells may either divide or transiently arrest from the cell cycle and invade [57], suggesting that the rate of proliferation is inversely proportional to invasion. Characterization of CD133⁻ve cells with HIF-1α displayed an upregulation in overall percentage and fluorescence intensity in compari-

son to the CD133⁺ve cells. Hypoxia (through HIF-1α activation) is also known to increase the expression of the *CXCR4* gene, a chemokine receptor associated with tumor progression and metastatic spread [58]. Therefore, the up-regulation of HIF-1α observed in our studies may contribute to the increased invasion seen in the CD133⁻ve cells.

Integrins are known to play a major role in cell adhesion to the ECM. It has been documented that, by decreasing oxygen, the levels of α_v integrin reduce [56]. This down-regulation of α_v revealed a mechanism by which hypoxia may inhibit adhesion. Characterization of the IN699 CD133⁺ve and CD133⁻ve populations with CD44, a receptor for hyaluronic acid, revealed low levels of antigen expression in both fractions. Similar findings where low oxygen levels downregulated the expression of cell adhesion molecules, including CD44, have also been reported [59]. Down-regulation of cellular adhesion may also cause integrin switching, enhancing the expression of integrins, which favor a particular development stage. Hypoxia may therefore induce remodeling of the ECM to favor invasion, as noted in our findings. Furthermore, the switching of integrins with regard to biologic activities demonstrated a positive correlation between adhesion and proliferation. To produce an increase in adhesion in all of the populations quantified, the ECM was also observed to induce an upregulated PI. If this is indeed correct, the proliferation data suggest that the IN699 CD133⁺ve cells are associated with β₁-integrin because of β-integrin's high association with adhesion and proliferation within this cellular fraction. β₁-Integrin–expressing cells also display positivity for the CD133 [60].

With increasing differentiation, the AC133 epitope decreases in a manner positively correlated with the loss of clonogenicity [61]. Moreover, in colon carcinoma cells, AC133 can be masked on cellular differentiation [61]. Consistent with these findings, Campos et al. [62] also reported a loss of AC133 immunoreactivity on differentiation without altering the CD133 mRNA. This suggests that protein folding may occur because of differential glycosylation, masking specific epitopes of CD133. Although this evidence suggests that CD133 expression is not restricted to CSC, it does imply that glycosylation supports the hierarchical model for tumor initiation. In addition, CD133⁻ve glioma cells have also been shown as capable of giving rise to CD133⁺ve cells [15], supporting our findings that CD133⁺ve and CD133⁻ve cells do not remain consistent in expression. Our data therefore suggest that, although on characterization with the AC133 antibody it seems there has been a "loss" of "stemness," differential glycosylation may actually take place, promoting not only differentiation but also an increased invasion propensity, until appropriate microconditions ensue for the AC133 epitope to present itself again. The CD133/1 (AC133) antigen has been identified as a glycosylated protein [63]. The mechanisms involved in tumor malignancy are maintained either directly or indirectly by *N*- or *O*-linked glycosylation or by the surrounding gangliosides [64]. Hakomori [65] demonstrated that CD133 can be saturated by gangliosides, thus affecting the phenotype of CD133. Both the IN699 CD133⁺ve and CD133⁻ve fractions displayed a high level of positivity for the ganglioside GD3, inferring that GD3 does not play a functional role in the biologic behavior of CD133. However, the amount of GD3 in the cell membrane at any one time may determine functional roles [66]. In contrast, it is highly likely that the glycosylation of the CD133 glycoprotein has a modulatory role in control of behavior. Alternatively, glycosylated CD133 (AC133) may sequester the GD3 antigen to the N-terminal of the protein, inducing the extracellular formation of endoglycosidases, resulting in the de-*N*-glycosylation of the CD133 molecule and the switching of integrin receptors, promoting

the invasive phenotype. Taïeb et al. [67] proposed that the extracellular N-terminal domain of the CD133 protein may undergo conformational alterations depending on the composition of membranous gangliosides, thus alterations in the membrane composition may be accountable for masking the AC133 epitope.

It has been suggested that tumorigenic CD133+ve cells are maintained in a dormant state but spontaneously enter the cell cycle to give rise to angiogenic CD133−ve daughter cells [45]. This implies that tumorigenesis is initiated by asymmetric cell divisions of the CD133+ve cells. However, on characterization of the IN699 CD133+ve fraction, we noted that almost all of the cells were Ki67-positive; therefore, one would assume that the CD133+ve cells are not maintained in a dormant state, at least under *in vitro* conditions. The spontaneous formation of CD133−ve cells might then support the stochastic tumor initiation model; hence, it is unlikely that the formation of either cell fraction is "spontaneous." The formation may in fact be determined by the microenvironment contributing to the differential glycosylation and reformation of the CD133 epitope. Our data suggest that the HIF-2α subunit contributes to the proliferation rate and maintenance of CD133+ve cells. Our data show that the CD133+ve and CD133−ve fractions are affected by different HIFs. During a 96-hour time course, from high- to low-oxygen tensions, the mean amount of HIF-1α antigen expression was observed to be inversely proportional to HIF-2α. Carroll and Ashcroft [68] also noted a down-regulation of HIF-2α in MCF-7 breast carcinoma cells, resulting in an up-regulation in HIF-1α–dependent vascular endothelial growth factor stimulation.

A number of previous studies have distinguished CD133+ve and CD133−ve cell populations in adult glioma based on their molecular signatures and phenotypic behavior [8,16,69,70]. In most cases, CD133+ve and CD133−ve cells had significantly different transcriptional profiles, generated either by global expression analysis or with a discrete panel of markers. However, differential genomic analysis of CD133+ve and CD133−ve factions has not been described in glioma. Our observation that IN699 CD133+ve and CD133−ve cells had identical genomic imbalances concurs with a recent report of indistinguishable array comparative genomic hybridization profiles in CD133+ve and CD133−ve isolates from colorectal carcinoma cell lines [70].

Our research documents a direct link between decreasing oxygen tension and glycosylated CD133 (AC133) expression. We have also shown that the *in vitro* hypoxic microenvironment facilitates a role in the *in vitro* behavior of pediatric GB cells. Therefore, the AC133 epitope of CD133 may characterize areas of low oxygen and an undifferentiated phenotype in tumor tissues, correlating with the radioresistance of tumor cells and the associate poor clinical outcome in patients [7,71]. In this article, we have reported a hitherto undocumented high expression of CD133+ve cells in a cultured pediatric GB that have been used further as a study model to investigate cellular biologic behavior and molecular profiles of CD133+ve and CD133−ve cells. Distinct biologic differences were obvious between the CD133+ve and CD133−ve cells fractions: 1) CD133−ve cells displayed an increased invasive propensity in comparison to the CD133+ve cells; 2) CD133+ve cells may be inversely linked to invasion, displaying an increased PI in comparison to CD133−ve cells; and 3) CD133 does not facilitate a role in cellular adhesion. However, our observations also indicated identical genomic imbalances between CD133+ve and CD133−ve fractions. Our results also suggest plasticity in CD133 expression. "Spontaneous" formation of the CD133 phenotype and microenvironmental influence suggests that CD133 is not a definitive brain tumor CSC marker. Its presence in pediatric GB may, however, significantly define biologic behavior and subsequent clinical outcome.

References

[1] Hemmati HD, Nakano I, Lazareff JA, Masterman-Smith M, Geschwind DH, Bronner-Fraser M, and Kornblum HI (2003). Cancerous stem cells can arise from paediatric brain tumours. *Proc Natl Acad Sci USA* **100**(25), 15178–15183.

[2] Brustle O and McKay RD (1995). The neuroepithelial stem cell concept: implications for neuro-oncology. *J Neurooncol* **24**(1), 57–59.

[3] Valtz NL, Hayes TE, Norregaard T, Liu SM, and McKay RD (1991). An embryonic origin for medulloblastoma. *New Biol* **3**(4), 364–371.

[4] Alvarez-Buylla A and Garcia-Verdugo JM (2002). Neurogenesis in adult subventricular zone. *J Neurosci* **22**(3), 629–634.

[5] Wechsler-Reya R and Scott MP (2001). The development biology of brain tumours. *Annu Rev Neurosci* **24**, 385–428.

[6] Corbeil D, Röper K, Hellwig A, Tavian M, Miraglia S, Watt SM, Simmons PJ, Peault B, Buck DW, and Huttner WB (2000). The human AC133 haematopoietic stem cell antigen is also expressed in epithelial cells and targeted to plasma membrane protrusions. *J Biol Chem* **275**(8), 5512–5520.

[7] Zeppernick F, Ahmadi R, Campos B, Dictus C, Helmke BM, Becker N, Lichter P, Unterberg A, Radlwimmer B, and Herold-Mende CC (2008). Stem cell marker CD133 affects clinical outcome in gliomas patients. *Clin Cancer Res* **14**(1), 123–129.

[8] Liu G, Yuan X, Zeng Z, Tunici P, Ng H, Abdulkadir IR, Lu L, Irvin D, Black KL, and Yu JS (2006). Analysis of gene expression and chemoresistance of CD133+ cancer stem cells in glioblastoma. *Mol Cancer* **5**, 67.

[9] Blazek ER, Foutch JL, and Maki G (2007). Daoy medulloblastoma cells that express CD133 are radioresistant relative to CD133− cells, and the CD133+ sector is enlarged by hypoxia. *Int J Radiat Oncol Biol Phys* **67**(1), 1–5.

[10] Bao S, Wu Q, McLendon RE, Hao Y, Shi Q, Hjelmeland AB, Dewhirst MW, Bigner DD, and Rich JN (2006). Glioma stem cells promote radioresistance by preferential activation of the DNA damage response. *Nature* **444**(7120), 756–760.

[11] Carmeliet P and Jain RK (2000). Angiogenesis in cancer and other diseases. *Nature* **407**(6801), 249–257.

[12] Kohshi K, Kinoshita Y, Imada H, Kunugita N, Abe H, Terashima H, and Tokui S (1999). Effects of radiotherapy after hyperbaric oxygenation on malignant glioma. *Br J Cancer* **80**(1–2), 236–241.

[13] Keith B and Simon MC (2007). Hypoxia-inducible factors, stem cells and cancer. *Cell* **129**(3), 465–472.

[14] Kaur B, Khwaja FW, Severson EA, Matheny SL, Brat DJ, and Van Meir EG (2005). Hypoxia and the hypoxia-inducible factor pathway in glioma growth and angiogenesis. *Neuro Oncol* **7**(2), 134–153.

[15] Wang J, Sakariassen PØ, Tsinkalovsky O, Immervoll H, Bøe SO, Svendsen A, Prestegarden L, Røsland G, Thorsen F, Stuhr L, et al. (2008). CD133 negative glioma cells form tumours in nude rats and give rise to CD133 positive cells. *Int J Cancer* **122**(4), 761–768.

[16] Beier D, Hau P, Proescholdt M, Lohmeier A, Wischhusen J, Oefner PJ, Aigner L, Brawanski A, Bogdahn U, and Beier CP (2007). CD133+ and CD133− glioblastoma-derived cancer stem cells show differential growth characteristics and molecular profiles. *Cancer Res* **67**(9), 4010–4015.

[17] Joo KM, Kim SY, Jin X, Song SY, Kong DS, Lee JI, Jeon JW, Kim MH, Kang BG, Jung Y, et al. (2008). Clinical and biological implications of CD133-positive and CD133-negative cells in glioblastomas. *Lab Invest* **88**(8), 808–815.

[18] Ward SJ, Karakoula K, Phipps KP, Harkness W, Hayward R, Thompson D, Jacques TS, Harding B, Darling JL, Thomas DG, et al. (2010). Cytogenetic analysis of paediatric astrocytoma using comparative genomic hybridisation and fluorescence *in-situ* hybridisation. *J Neurooncol* **98**, 305–318.

[19] Csete M (2005). Oxygen in the cultivation of stem cells. *Ann N Y Acad Sci* **1049**, 1–8.

[20] Sullivan M, Galea P, and Latif S (2006). What is the appropriate oxygen tension for *in vitro* culture? *Mol Hum Reprod* **12**(11), 653.

[21] Cheng JX, Liu BL, and Zhang X (2009). How powerful is CD133 as a cancer stem cell marker in brain tumours? *Cancer Treat Rev* **35**(5), 403–408.

[22] Pilkington GJ (2005). Cancer stem cells in the mammalian central nervous system. *Cell Prolif* **38**(6), 423–433.

[23] Vescovi AL, Galli R, and Reynolds BA (2006). Brain tumour stem cells. *Nat Rev Cancer* **6**(6), 425–436.

[24] Sakakibara S, Imai T, Hamaguchi K, Okabe M, Aruga J, Nakajima K, Yasutomi D, Nagata T, Kurihara Y, Uesugi S, et al. (1996). Mouse-Musashi-1, a neural RNA-binding protein highly enriched in the mammalian CNS stem cell. *Dev Biol* **176**(2), 230–242.

[25] Uchida K, Mukai M, Okano H, and Kawase T (2004). Possible oncogenicity of subventricular zone neural stem cells: case report. *Neurosurgery* **55**(4), 977–978.

[26] Thon N, Damianoff K, Hegermann J, Grau S, Krebs B, Schnell O, Tonn JC, and Goldbrunner R (2010). Presence of pluripotent CD133+ cells correlates with malignancy of gliomas. *Mol Cell Neurosci* **43**(1), 51–59.

[27] Okano H, Imai T, and Okabe M (2002). Musashi: a translational regulator of cell fate. *J Cell Sci* **115**(7), 1355–1359.

[28] Kanemura Y, Mori K, Sakakibara S, Fujikawa H, Hayashi H, Nakano A, Matsumoto T, Tamura K, Imai T, Ohnishi T, et al. (2001). Musashi1, an evolutionary conserved neural RNA-binding protein, is a versatile marker of human glioma cells in determining their cellular origin, malignancy, and proliferative activity. *Differentiation* **68**(2–3), 141–152.

[29] Zhang M, Song T, Yang L, Chen R, Wu L, Yang Z, and Fang J (2008). Nestin and CD133: valuable stem cell–specific markers for determining clinical outcome of glioma patients. *J Exp Clin Cancer Res* **27**, 85.

[30] Lendahl U, Zimmerman LB, and McKay RD (1990). CNS stem cells express a new class of intermediate filament protein. *Cell* **60**(4), 585–595.

[31] Thomas SK, Messam CA, Spengler BA, Biedler JL, and Ross RA (2004). Nestin is a potential mediator of malignancy in human neuroblastoma cells. *J Biol Chem* **279**(27), 27994–27999.

[32] Ligon KL, Huillard E, Mehta S, Kesari S, Liu H, Alberta JA, Bachoo RM, Kane M, Louis DN, Depinho RA, et al. (2007). Olig2-regulated lineage-restricted pathway controls replication competence in neural stem cells and malignant glioma. *Neuron* **53**(4), 503–517.

[33] Azzarelli B, Miravalle L, and Vidal R (2004). Immunolocalisation of the oligodendrocyte transcription factor 1 (Olig 1) in brain tumours. *J Neuropathol Exp Neurol* **63**(2), 170–179.

[34] Bouvier C, Bartoli C, Aquirre-Cruz L, Virad I, Colin C, Fernandez C, Gouvernet J, and Figarella-Branger D (2003). Shared oligodendrocyte lineage gene expression in gliomas and oligodendrocyte progenitor cells. *J Neurosurg* **99**(2), 344–350.

[35] Lgon KL, Alberta JA, Kho AT, Weiss J, Kwann MR, Nutt CL, Louis DN, Stiles CD, and Rowitch DH (2004). The oligodendroglial lineage marker OLIG2 is universally expressed in diffuse gliomas. *J Neuropathol Exp Neurol* **63**(5), 499–509.

[36] Marie Y, Sanson M, Mokhtari K, Leuraud P, Kujas M, Delattre JY, Poirier J, Zalc B, and Hoang-Xuan K (2001). OLIG2 as a specific marker of oligodendroglial tumour cells. *Lancet* **358**(9278), 298–300.

[37] Kippin TE, Martens DJ, and Van der Kooy D (2005). p21 loss compromises the relative quiescence of forebrain stem cell proliferation leading to exhaustion of their proliferation capacity. *Genes Dev* **19**(6), 756–767.

[38] Gangemi RM, Grifffero F, Marubbi D, Perera M, Capra MC, Malatesta P, Ravetti GL, Zona GL, Daga A, and Corte G (2009). Sox2 silencing in glioblastoma tumour-initiating cells causes stop of proliferation and loss of tumourigenicity. *Stem Cells* **27**(1), 40–48.

[39] Rodriguez-Pinilla SM, Sarrio D, Moreno-Bueno G, Rodriguez-Gil Y, Martinez MA, Hernandez L, Hardisson D, Reis-Filho JS, and Palacios J (2007). Sox2: a possible driver of the basal-like phenotype in sporadic breast cancer. *Mod Pathol* **20**(4), 474–481.

[40] Schmitz M, Temme A, Senner V, Ebner R, Schwind S, Stevanovic S, Wehner R, Schackert G, Schackert HK, Fussel M, et al. (2007). Identification of SOX2 as a novel glioma-associated antigen and potential target for T cell–based immunotherapy. *Br J Cancer* **96**(8), 1293–1301.

[41] Gu G, Yuan J, Wills M, and Kasper S (2007). Prostate cancer cells with stem cell characteristics reconstitute the original human tumour *in vivo*. *Cancer Res* **67**(10), 4807–4815.

[42] Phi JH, Park SH, Paek SH, Kim SK, Lee YJ, Park CK, Cho BK, Lee DH, and Wang KC (2007). Expression of Sox2 in mature and immature teratomas of central nervous system. *Mod Pathol* **20**(7), 742–748.

[43] Spisek R, Kukreja A, Chen LC, Matthews P, Mazumder A, Vesole D, Jagannath S, Zebroski HA, Simpson AJ, Ritter G, et al. (2007). Frequent and specific immunity to the embryonal stem cell–associated antigen SOX2 in patients with monoclonal gammopathy. *J Exp Med* **204**(4), 831–840.

[44] Otsubo T, Akiyama Y, Yanagihara K, and Yuasa Y (2008). SOX2 is frequently downregulated in gastric cancers and inhibits cell growth through cell-cycle arrest and apoptosis. *Br J Cancer* **98**(4), 831–840.

[45] Liu Q, Nguyen DH, Dong Q, Shitaku P, Chung K, Liu OY, Tso JL, Liu JY, Konkankit V, Cloughesy TF, et al. (2009). Molecular properties of CD133+ glioblastoma stem cells derived from treatment-refractory recurrent brain tumours. *J Neurooncol* **94**(1), 1–19.

[46] Son MJ, Woolard K, Nam DH, Lee J, and Fine HA (2009). SSEA-1 is an enrichment marker for tumour-initiating cells in human glioblastoma. *Cell Stem Cell* **4**(5), 440–452.

[47] Martin K, Akinwunmi J, Rooprai HK, Kennedy AJ, Linke A, Ognjenovic N,

[48] Rebetz J, Tian D, Persson A, Widegren B, Salford LG, Englund E, Gisselsson D, and Fan X (2008). Glial progenitor-like phenotype in low-grade glioma and enhanced CD133-expression and neuronal lineage differentiation potential in high-grade glioma. *PLoS One* **3**(4), e1936.

[49] Sanai N, Alvarez-Buylla A, and Berger MS (2005). Neural stem cells and the origin of gliomas. *N Engl J Med* **353**(8), 811–822.

[50] Chekenya M and Pilkington GJ (2002). NG2 precursor cells in neoplasia: functional, histogenesis and therapeutic implications for malignant brain tumours. *J Neurocytol* **31**(6–7), 507–521.

[51] Buick RN, Minden MD, and McCulloch EA (1979). Self-renewal in culture of proliferative blast progenitor cells in acute myeloblastic leukaemia. *Blood* **54**(1), 95–104.

[52] Holland EC, Celestino J, Dai C, Schaefer L, Sawaya RE, and Fuller GN (2000). Combined activation of Ras and Akt in neural progenitors induces glioblastoma formations in mice. *Nat Genet* **25**(1), 55–57.

[53] Gustafsson MV, Zheng X, Pereira T, Gradin K, Jin S, Lundkvist J, Ruas JL, Poellinger L, Lendahl U, and Bondesson M (2005). Hypoxia requires notch signalling to maintain the undifferentiated cell state. *Dev Cell* **9**(5), 617–628.

[54] Gordan JD, Bertout JA, Hu CJ, Diehl JA, and Simon MC (2007). HIF2-α promotes hypoxic cell proliferation by enhancing c-*myc* transcriptional activity. *Cancer Cell* **11**(4), 335–347.

[55] Patel SA and Simon MC (2008). Biology of hypoxia-inducible factor-2α in development and disease. *Cell Death Differ* **15**(4), 628–634.

[56] Lash GE, Fitzpatrick TE, and Graham CH (2001). Effect of hypoxia on cellular adhesion to vitronectin and fibronectin. *Biochem Biophys Res Commun* **287**(3), 622–629.

[57] Pilkington GJ (1994). Tumour cell migration in the central nervous system. *Brain Pathol* **4**(2), 157–166.

[58] Staller P, Sulitkova J, Lisztwan J, Moch H, Oakeley EJ, and Krek W (2003). Chemokine receptor CXCR4 downregulated by von Hippel–Lindau tumour suppressor pVHL. *Nature* **425**(6955), 307–311.

[59] Hasan NM, Adams GE, Joiner MC, Marshall JF, and Hart IR (1998). Hypoxia facilitates tumour cell detachment by reducing expression of surface adhesion molecules and adhesion to extracellular matrices without loss of viability. *Br J Cancer* **77**(11), 1799–1805.

[60] Hall PE, Lathita JD, Miller NG, Caldwell MA, and Ffrench-Constant C (2006). Integrins are markers of human neural stem cells. *Stem Cells* **24**(9), 2078–2084.

[61] Kemper K, Sprick MR, de Bree M, Scope A, Vermeulen L, Hoek M, Zeilstra J, Pals ST, Mehmet H, Stassi G, et al. (2010). The AC133 epitope, but not the CD133 protein, is lost upon cancer stem cell differentiation. *Cancer Res* **70**(2), 719–729.

[62] Campos B, Zeng L, Daotrong PH, Eckstein V, Unterberg A, Mairbäurl H, and Herold-Mende C (2011). Expression and regulation of AC133 and CD133 in glioblastoma. *Glia* **59**(12), 1974–1986.

[63] Yin AH, Miraglia S, Zanjani ED, Almeida-Porada G, Ogawa M, Leary AG, Olweus J, Kearney J, and Buck DW (1997). AC133, a novel marker for human haematopoietic stem and progenitor cells. *Blood* **90**(12), 5002–5012.

[64] Ono M and Hakomori S (2004). Glycosylation defining cancer cell motility and invasiveness. *Glycoconj J* **20**(1), 71–78.

[65] Hakomori S (1996). Tumour malignancy defined by aberrant glycosylation and sphingo(glycol)lipid metabolism. *Cancer Res* **56**(23), 5309–5318.

[66] Birks SM, Danquah JO, King L, Vlasak R, Gorecki DC, and Pilkington GJ (2011). Targeting the GD3 acetylation pathway selectively induces apoptosis in glioblastoma. *Neuro-oncology* **13**(9), 950–960.

[67] Taïeb N, Maresca M, Guo XJ, Garmy N, Fantini J, and Yahi N (2009). The first extracellular domain of the tumour stem cell marker CD133 contains an antigenic ganglioside-binding motif. *Cancer Lett* **278**(2), 164–173.

[68] Carroll VA and Ashcroft M (2006). Role of hypoxia-inducible factor (HIF)-1α *versus* HIF-2α in the regulation of HIF target genes in response to hypoxia, insulin-like growth factor-I, or loss of von Hippel–Lindau function: implications for targeting the HIF pathway. *Cancer Res* **66**(12), 6264–6270.

[69] Lottaz C, Beier D, Meyer K, Kumar P, Hermann A, Schwarz J, Junker M, Oefner PJ, Bogdahn U, Spang R, et al. (2010). Transcriptional profiles of CD133+ and CD133− glioblastoma-derived cancer stem cell lines suggest different cells of origin. *Cancer Res* **70**(5), 2030–2040.

[70] Gaiser T, Camps J, Meinhardt S, Wangsa D, Nguyen QT, Varma S, Dittfield C, Kunz-Schughart LA, Kemmerling R, Becker MR, et al. (2011). Genome and transcriptome profiles of CD133-positive colorectal cancer cells. *Am J Pathol* **178**, 1478–1488.

[71] Wan F, Herold-Mende C, Campos B, Centner FS, Dictus C, Becker N, Devens F, Mogler C, Felberg J, Grabe N, et al. (2011). Association of stem cell–related markers and survival in astrocytic gliomas. *Biomarkers* **16**(2), 136–143.

and Pilkington GJ (1995). Nonexpression of CD15 by neoplastic glia: a barrier to metastasis? *Anticancer Res* **15**(4), 1159–1166.

Table W1. Genomic Losses and Gains in IN699.

Cytoband Location	Event	Region Length (bp)	Genes
1p36.33	CN gain	596,963	11
1p36.11 – p33	CN gain	21,599,034	334
1p33 – p32.3	CN gain	5,086,703	58
1p31.1 – q11	CN gain	47,102,085	302
1q21.1 – q21.3	CN gain	5,989,293	135
1q21.3 – q23.1	CN gain	4,654,974	148
1q25.3	CN gain	3,653,976	30
1q31.3 – q32.1	CN gain	8,003,229	107
1q32.1 – q42.11	CN loss	17,363,747	107
1q42.12 – q44	CN loss	17,861,791	115
1q44	CN loss	3,504,889	66
2p25.3 – p25.2	CN loss	6,150,286	22
2p23.3 – p23.2	CN gain	2,403,889	38
2p22.3 – p16.3	CN gain	12,807,038	83
2p16.2 – p16.1	CN gain	3,492,096	27
2p16.1 – p12	CN gain	17,740,336	143
2p12 – p11.2	CN gain	6,370,822	55
2q11.1 – q14.1	CN gain	21,598,724	176
2q14.1 – q14.3	CN gain	7,007,493	25
2q14.3	CN gain	4,061,048	18
2q21.3	CN gain	223,691	4
2q24.1 – q24.2	CN gain	6,252,983	25
2q24.3 – q32.2	CN gain	24,640,768	136
3p26.3 – p24.3	CN loss	14,969,624	94
3p24.3	CN gain	153,663	3
3p24.3 – p21.31	CN loss	31,734,929	184
3p14.3 – q11.1	CN loss	33,801,099	73
3q11.2 – q12.2	CN loss	7,399,778	39
4p16.3 – p14	CN loss	37,951,466	189
4p13 – q32.3	CN loss	127,882,623	527
4q32.3	CN gain	233,115	2
4q32.3 – q35.2	CN loss	21,518,428	129
5p15.33	CN gain	3,603,755	34
5p13.3 – p13.1	CN gain	8,723,688	50
5q12.3 – q14.3	CN loss	22,947,949	143
5q33.3 – q35.2	CN gain	19,053,329	99
5q35.3	CN gain	3,802,280	63
6p25.3 – p24.2	CN loss	10,841,147	65
6p11.2 – q11.1	CN loss	3,207,171	2
6q11.1	CN gain	1,559,394	0
6q11.1 – q12	CN loss	7,643,209	8
6q14.1	CN loss	4,575,744	10
6q21	CN gain	1,047,103	8
6q21	CN gain	517,159	5
7p21.2 – p21.1	CN gain	1,478,677	3
7p15.2 – p15.1	CN gain	3,145,415	28
7p14.1 – p12.3	CN gain	7,550,255	59
7q11.22	CN gain	662,999	1
7q11.23 – q21.11	CN gain	12,666,389	89
7q35	CN loss	669,336	1
8p23.1	CN gain	4,407,582	76
8p23.1 – q11.21	CN gain	36,438,850	205
8q13.1 – q21.11	CN gain	7,585,870	41
8q21.12 – q21.13	CN gain	3,666,688	17
8q21.3 – q23.1	CN gain	15,423,079	82
8q23.3 – q24.22	CN gain	15,893,204	66
8q24.3	CN gain	6,101,253	114
9p24.3 – p21.1	CN loss	28,461,665	116
9p13.1 – q11	CN loss	12,872,313	35
9q21.33	CN gain	829,222	5
9q22.2 – q31.1	CN gain	10,284,608	107
9q31.3 – q33.1	CN gain	6,533,593	63
9q33.2 – q34.3	CN gain	18,005,802	329
10p12.1 – p11.23	CN gain	385,701	2
10q11.21 – q11.22	CN loss	5,683,600	62
10q21.3	CN loss	237,262	1
11p15.4	CN gain	1,179,717	21
11p15.2 – p15.1	CN gain	3,077,089	34
11p11.2 – p11.12	CN loss	3,161,065	15
11q14.1	CN loss	4,925,671	11
11q14.3	CN loss	548,824	3
11q21	CN gain	1,213,132	6
11q23.3 – q25	CN loss	15,945,313	134

Table W1. (*continued*)

Cytoband Location	Event	Region Length (bp)	Genes
12p13.33 – q12	CN loss	41,094,862	336
12q14.1	CN loss	1,462,517	1
12q14.1 – q14.3	CN gain	3,499,207	20
12q24.31	CN gain	788,508	13
12q24.31	CN gain	1,899,515	24
13q11 – q12.3	CN loss	12,957,921	74
13q14.11 – q21.2	CN gain	15,927,992	110
13q21.2 – q31.1	CN loss	25,539,125	40
13q31.1	CN gain	52,493	1
13q31.1 – q31.3	CN gain	6,427,744	13
13q31.3 – q34	CN loss	21,435,167	96
14q11.1 – q13.1	CN loss	13,971,938	171
14q22.1	CN gain	1,600,129	20
14q23.2 – q23.3	CN loss	4,308,546	27
14q32.33	CN loss	1,513,172	11
15q11.2	CN loss	1,512,134	15
15q11.2 – q22.31	CN loss	41,678,197	449
15q24.1	CN gain	333,787	4
15q25.1 – q25.2	CN loss	3,270,540	30
15q26.3	CN gain	44,315	3
15q26.3	CN loss	666,735	11
16p13.3	CN gain	850,396	13
16p11.2	CN loss	2,045,883	10
16q21	CN loss	4,674,102	1
16q22.2	CN loss	337,574	1
17p13.3	CN loss	2,947,228	54
17p13.3 – p13.1	CN gain	7,226,737	197
17p12 – p11.2	CN gain	5,845,900	93
17p11.2 – p11.1	CN loss	1,620,116	12
17p11.1 – q11.1	CN gain	95,705	0
17q11.1 – q12	CN loss	7,794,880	111
17q25.1 – q25.2	CN gain	440,781	17
17q25.2 – q25.3	CN loss	6,376,544	115
18p11.32 – p11.31	CN loss	3,009,422	19
18p11.31 – q11.1	CN loss	12,249,665	55
18q11.2 – q22.2	CN loss	47,462,351	188
18q22.3 – q23	CN loss	9,205,484	32
19p13.3	CN gain	243,848	6
19p13.3	CN loss	3,334,196	121
19p13.11 – q11	CN loss	9,743,747	70
19q12 – q13.2	CN loss	13,538,594	237
19q13.31	CN loss	729,970	16
19q13.41	CN loss	1,110,621	31
20p11.21 – p11.1	CN gain	827,582	11
20p11.1 – q11.21	CN loss	3,551,079	5
20q13.2 – q13.33	CN gain	8,923,757	134
21p11.2 – q11.1	CN loss	2,403,370	6
21q22.2 – q22.3	CN loss	1,442,348	9
22q13.31 – q13.33	CN loss	3,810,101	45
Xq23 – q26.3	CN gain	18,509,992	166
Yp11.32 – q11.23	CN loss	27,177,529	191
Yq12	CN loss	395,226	3